Combined Utilization of Construction and Demolition Waste and Propylene Fiber in Cement-Stabilized Soil

Genbao Zhang [1], Zhiqing Ding [2], Runhong Zhang [2,3], Changfu Chen [4,5], Guihai Fu [1,6], Xiao Luo [1], Yufei Wang [7,*] and Chao Zhang [8]

1   College of Civil Engineering, Hunan City University, Yiyang 413000, China; genbao@hncu.edu.cn (G.Z.); fuguihai@hncu.edu.cn (G.F.); luoxiao@hncu.edu.cn (X.L.)
2   Institute for Smart City of Chongqing University in Liyang, Chongqing University, Liyang 213300, China; 22390016@student.uwa.edu.au (Z.D.); zhangrh@cqu.edu.cn (R.Z.)
3   College of Aerospace Engineering, Chongqing University, Chongqing 400045, China
4   Key Laboratory of Building Safety and Energy Efficiency of the Ministry of Education, Hunan University, Changsha 410082, China; cfchen@hnu.edu.cn
5   College of Civil Engineering, Hunan University, Changsha 410082, China
6   Hunan Engineering Research Center of Structural Safety and Disaster Prevention for Urban Underground Infrastructure, Yiyang 413000, China
7   School of Design and Built Environment, Curtin University, Bentley, WA 6102, Australia
8   College of Civil Engineering, Hunan University of Science and Technology, Xiangtan 411100, China; flyheartzc@hnust.edu.cn
*   Correspondence: wangyf0113_suz@163.com

Abstract: Construction and demolition (C&D) waste has become a research hotspot due to the need for environmental sustainability and strength enhancement of cementitious materials. However, wider applications of C&D waste are limited, as its non-homogeneous surface nature limits its workability. This research evaluated the feasible utilization of C&D waste as aggregates in polypropylene-fiber-reinforced cement-stabilized soil (CSS) under sulfate-alkali activation. CSS specimens incorporated Portland cement and C&D waste in 10%, 20%, and 30% proportions. Also, polypropylene fiber after alkali activation by sodium sulfate (at 0.2%, 0.4%, and 0.8% dosing level) was defined as 1%, 2%, and 4%. Strength enhancement was examined through unconfined compressive strength (UCS) and flexural strength tests at 7, 14 and 28 days. Test results indicated that mechanical properties showed significant improvement with increasing levels of Portland cement and sodium sulfate, while the improvement dropped after excessive addition of C&D waste and polypropylene fiber. Optimal proportioning was determined as 30%, 4%, 20%, and 0.8% for Portland cement, polypropylene fiber, C&D waste, and sodium sulfate, respectively. Scanning electron microscope (SEM) analysis attributed the enhancement to hydration product (ettringite) formation, bridging effect and increased particle friction. Additionally, the decrease in amplification was ascribed to the destruction of interface transition-zone (ITZ) strength, resulting in premature failure.

Keywords: alkali activation; cement-stabilized soil; waste utilization; fiber-reinforced soil; SEM analysis; mechanical property; optimum design

1. Introduction

The rapid development of infrastructure has released numerous construction and demolition (C&D) waste, reaching an annual production of 3039 Mt in China alone [1]. However, solid waste resourcing is still not globally applied, with utilization rates varying dramatically from 5–90%, resulting in resource waste and environmental pollution [2–4]. Specifically, the construction process generates greenhouse gas emissions along with solid waste, leading to climate change and soil erosion [5,6]. The sustainable lifecycle of construction activity has therefore become essential to creating eco-friendly architecture [7,8]. C&D waste utilization yields application potentials including aggregates in cementitious

materials and road base materials (embankment, subbase and asphalt pavement) [9,10]. Through grinding–incineration treatment, C&D waste presents enhanced bonding properties with the binding mixture [11,12]. Moreover, as the production of cement generates up to 7% of its carbon footprint, utilizing C&D waste tackles the problem with the benefits of waste utilization and cement usage reduction [13]. However, C&D waste shows weaker performance, owing to the wall effect and a further quantity of cracks [14–17]. Old interface transition zones (ITZs) in C&D waste exhibit weaker strength, becoming highly prone to cracks. Simultaneously, C&D waste weakens density and durability, despite its advantages in abrasion resistance [18–20]. As a result, the replacement threshold limitation for natural aggregate is concluded as being 50% with scarified compressive strength [21–23]. Application strategies maximizing the potential of C&D waste have therefore become a research hotspot that has been extensively explored.

The use of C&D waste as aggregates in cement-stabilized soil (CSS) for foundations has been reported as a rapidly emerging method [24–26]. CSS demonstrates outstanding suitability, due to its economic effect and simple operation, which can be further enhanced while being prepared in situ [27,28]. The application fields include foundation treatments, leakage-stopping and slope reinforcement, where large quantities of low strength materials are required [29]. As a result, the 50% threshold limitation can be exceeded. The widely sourced soil incorporated in CSS varies from sand, coal gangue, and volcanic slag to ground concrete, which enables the material to satisfy the demand for in situ preparation.

In addition, C&D waste represents positive coupling with sulfate dosage. First, C&D waste particles further develop performance enhancement provided by sulfate. Two previous studies on salt activators have proved the SO_4^{2-} ions as superior hydration catalysts, reducing the initial and final setting time of CSS by 81.1% and 67.8%, respectively [30,31]. Meanwhile, cations (such as Na^+, Ca^{2+}) fulfill the function of alkalinities, forming more dispersed glassy phases [32]. C&D waste particles therefore form a compact structure with the binder, resulting in significant improvement in compressive strength. Second, C&D waste demonstrates resistance to sulfate erosion. Sulfate attack becomes a bigger issue as salt proportion increases, which leads to large-scale sulfate heaving, cracking, and structure failure [33,34]. Tang et al. [35] claimed that C&D waste inhibited the degree of sulfate erosion and remarkably strengthened the durability.

However, the poor cracking resistance and shrinkage deformation often present hindrances in the wider application of C&D waste in CSS. Proven enhancements include chemical additives, such as lime and cement in the stabilized soil matrix, but the enhanced blocks are prone to cracking and sudden failure [36–38]. To the authors' knowledge, previous literature demonstrates the mitigation provided by increased cement blending [39,40]. However, sulfate erosion depends on many more factors (pH, temperature, aggregates, etc.) [41]. The coupling has not yet been clearly assessed, which therefore suggests numerous potential scopes for machine-learning research [42–45].

Fibrous materials were introduced to improve the mechanical properties in this scenario, bringing intersecting and bridging effects to the mixture. The randomly distributed fiber yields the benefits of crack reduction and unconfined compressive strength (UCS) increments [46]. An increase of up to 115% in UCS was observed in the experimental study, and the strength can be further enhanced by switching fiber types [47–50]. Polypropylene fiber showed resistance against sulfate deterioration. Mixtures with polypropylene fiber inclusion exhibit higher porosity, which allows more space for expansion and consequent hydrate-phase (gypsum and ettringite) formation [51–53]. Previous literature includes numerous studies on fiber-reinforcement treatment. However, its combination with the use of C&D waste has rarely been investigated.

This research presents the mechanical enhancement of CSS by the combination of C&D waste and polypropylene fiber. Portland cement 42.5 was employed to provide better stabilization and mechanical performance. Testing variables include admixture of cement, C&D waste, fiber, and sodium sulfate. Apart from the compressive and flexural strength test, scanning electron microscope (SEM) analysis was conducted to examine the

proposed mixture. Ultimately, an optimum mixture design was selected according to the experimental analysis.

2. Materials and Experimental Program

2.1. Materials Selection

The soil for this research was collected from the under-construction metro station Zhushan Road of line 5 in Nanjing, and consisted of silty clay taken from 12 m below the surface. Tables 1 and 2 list the mechanical properties and composition of the soil sample. Polypropylene fiber was chosen for this research, owing to its superior tensile strength, chemical stability, and dispersibility. Table 3 shows the performance specifications of the polypropylene fiber. C&D waste was collected from a construction site in Nanjing containing waste masonry blocks, fine sand, and gravel. Particles were ground and sieved to a size less than 5 mm. Portland cement 42.5 and sodium sulfate were used as cemental binder and alkali catalyst, respectively. The tests were carried out with strict reference to GB/T50123-1999 [54].

Table 1. Physical and mechanical properties of soil sample.

Soil Properties	Value
Specific gravity	2.69
Liquid limit (%)	38.87
Plastic limit (%)	21.55
Plasticity index	17.32
Maximum dry density (g/cm^3)	1.51
Optimum moisture content (%)	25.37

Table 2. Concentration of composition in sample soil.

Composition	Concentration Value
Sand	17.8%
Silt	64.6%
Clay	17.5%
Mineral Composition	**Concentration Value**
Quartz	33.8%
Kaolinite	52.4%
Montmorillonite	1.3%
Elixirite	7.6%
Calcite	2.1%
Organic matter	2.9%

Table 3. Physical and mechanical properties of polypropylene fiber.

Polypropylene Fiber Properties	Value
Diameter (μm)	10
Cut length (mm)	10
Density (g/cm^3)	0.91
Tensile strength (MPa)	486
Stretching limit (%)	15
Acid resistance	Excellent
Alkali resistance	Excellent

2.2. Mixture Design

The adopted testing variable included the dosage of fiber, C&D waste, sodium sulfate and cement. The content of water was kept constant at 80%. Other contents were defined

from Equation (1), where a is the abbreviation for admixture and W is the weight of pre-dried soil.

$$\rho_a = \frac{W_a}{W} \tag{1}$$

Specifically, Portland cement and C&D waste were used at 10%, 20% and 30%. Dosing level of fiber was 1%, 2%, 4% and of sodium sulfate was 0.2%, 0.4%, 0.8% among total weight. Table 4 provides the mixing percentages for each variable. The integrated mixture design resulted in 81 combinations of variables along 3 control groups. The specified mixture design is shown in the Appendix A.

Table 4. Testing variables and proportion.

Testing Variable	Proportion
42.5 Portland cement	10%; 20%; 30%
Polypropylene fiber	1%; 2%; 4%
C&D waste	10%; 20%; 30%
Sodium sulfate	0.2%; 0.4%; 0.8%
Water	80%

2.3. Specimen Preparation

The specimens were prepared in accordance with GB/T50123-1999 [54], identifying with the mixing design presented in Table 4. Pre-dried soil and C&D waste were adequately ground and sieved to ensure similar gradations. Meanwhile, fiber agglomeration was avoided by air gun pretreatment and batch incorporation. Specifically, the high-pressure gas ejected from the air gun blew the polypropylene fiber towards the mortar. Fibers were grouped into small clusters to avoid weakening the inhibition of agglomeration due to excessive dosing at one time. The concocted soil-cement mixture was injected into the mold and vibrated to expel entrapped air. The samples were then wrapped in clean film and placed in the curing chamber for standard curing (temperature (20 ± 2) °C, relative humidity above 95%) until the test was conducted. Three replicated samples were prepared for each variable combination to conduct the compressive and flexural strength test.

2.4. Testing Procedure

Mechanical performance was evaluated in this research conforming to GB/T50123-1999 [54]. The sample dimensions for UCS and flexural strength test were kept consistent with the protocol as 50 mm $\times$ 50 mm $\times$ 50 mm and 40 mm $\times$ 40 mm $\times$ 160 mm, respectively. Tests were carried out at 7, 14, and 28 days of curing age. The day before the compressive performance evaluation, specimens were removed from the curing conditions and immersed in water at 24 °C for 24 h to simulate a real working environment. All laboratory tests were conducted by YAW-4206 and DY-208JX automatic pressure testers at a strain rate of 0.04 MPa/s until failure occurs.

SEM analysis was conducted to explore the modification of CSS at the microstructure level with the inclusion of polypropylene fiber, cement, C&D waste, and sodium sulfate. The fracture surface of UCS was cut into pieces measuring 1 cm $\times$ 1 cm $\times$ 1 cm to be observed.

3. Results and Discussion

3.1. Unconfined Compressive Strength Test

Figure 1 depicts the UCS test results of the control groups, indicating the performance enhancement by increasing Portland cement dosage and curing age. It can be observed that cement inclusion improved the strength of soil at all curing ages, while the maximum 28 d improvement reached 153.44%. The enhancement was attributed to more cement hydration products. When the cement content increases gradually, the consequent calcium silicate ($CaSiO_3$) and C-S-H gel fill the porosity and significantly improve the compressive

strength [55,56]. Simultaneously, UCS increases rapidly in the early curing stage (7–14 d), and the growth rate slowed down with time. The maximum increments from 7 to 14 days and 14 to 28 days curing stage were 185.73% and 36.18%, respectively, indicating the hydration products promoted the increase in bonding strength between cement and soil particles. At the curing age of 28 days, the hydration reaction was thorough, and the strength of the sample gradually stabilized to maintain a stable value.
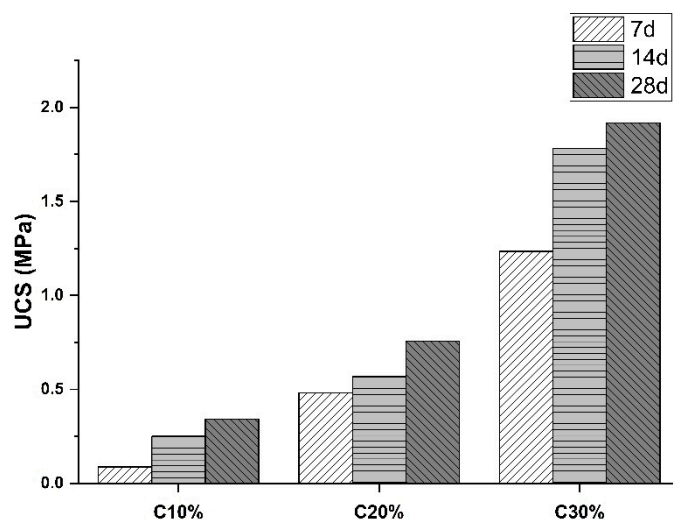

Figure 1. Compressive strength enhancement for the control group (Note: C represents Portland cement).

However, Portland cement introduced an undesired failure mode as well. A brittle fracture surface was observed after the UCS test, presenting a distinct oblique shear plane. The failure occurred without obvious signs beforehand, which resulted in soil spalling and form damage. The effect can be ascribed to the alkali–silica reaction (ASR), which indicates that Portland cement increases the material's brittleness [57–59]. Therefore, the specimen cannot be deformed in response to external forces.

Figure 2 shows the UCS results for specimens dosed with 10% cement, while Figure 2a–c are divided into the C&D waste dosing levels of 10%, 20% and 30%. Figures 3 and 4 illustrate the UCS of specimens with 20% and 30% cement under the same logic. It is evident in Figures 2 and 3 that polypropylene fiber inclusion increases UCS performance. This can be ascribed to the inhibitory characteristics of fiber against sudden failure. With increased percentage, polypropylene fibers form spatial network-like structures and bridging effects in CSS slurry, which gradually inhibit crack generation [60,61]. The fiber bridge can additionally produce deformation constraints when the sample cracks. Moreover, polypropylene fiber provides higher movement resistance than that between soil particles [62]. Given that, the friction impedes particle displacement in the CSS specimen, which further exploits the strength enhancement among external forces. However, as in Figure 4c, a 31.52% degeneration was noticed. This was because with the cement dosage rising, the decrease in sample compactness caused by excessive fiber incorporation could no longer be neutralized by soil and C&D waste [63,64]. As observed in microstructure analysis, numerous fiber/binder ITZs appeared in the CSS, which significantly impaired the bonding strength. Notably, the compressive strength again grew significantly at 0.8% sodium sulfate in Figure 4c from 2–4% fiber dosage. This may be ascribed to sodium sulfate activating the formation of hydration products, providing strength and fewer air voids and thereby compensating for the reduction.
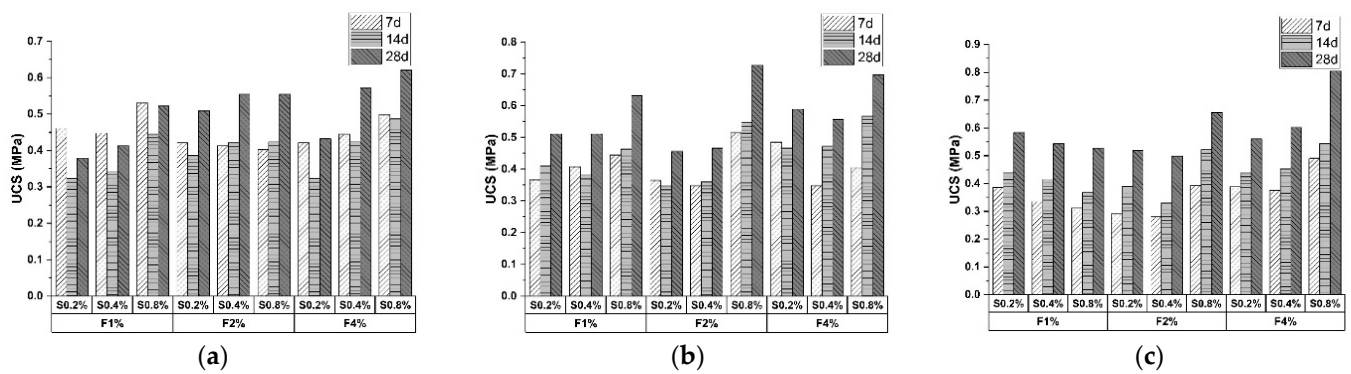
Figure 2. Unconfined compressive strength of 10% cement specimen with (**a**) 10% C&D waste; (**b**) 20% C&D waste; (**c**) 30% C&D waste (Note: S represents sodium sulfate; F represents polypropylene fiber).

Figure 3. Unconfined compressive strength of 20% cement specimen with (**a**) 10% C&D waste; (**b**) 20% C&D waste; (**c**) 30% C&D waste (Note: S represents sodium sulfate; F represents polypropylene fiber).
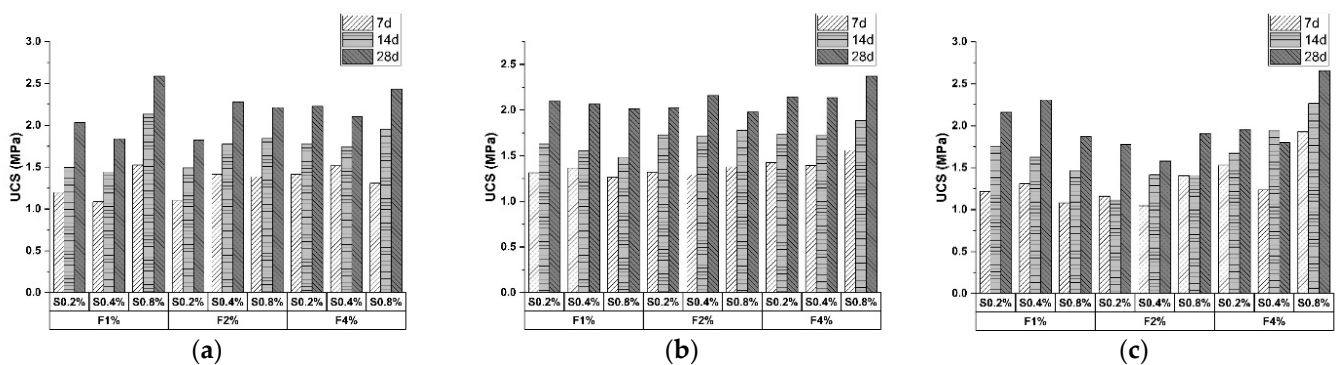
Figure 4. Unconfined compressive strength of 30% cement specimen with (**a**) 10% C&D waste; (**b**) 20% C&D waste; (**c**) 30% C&D waste (Note: S represents sodium sulfate; F represents polypropylene fiber).
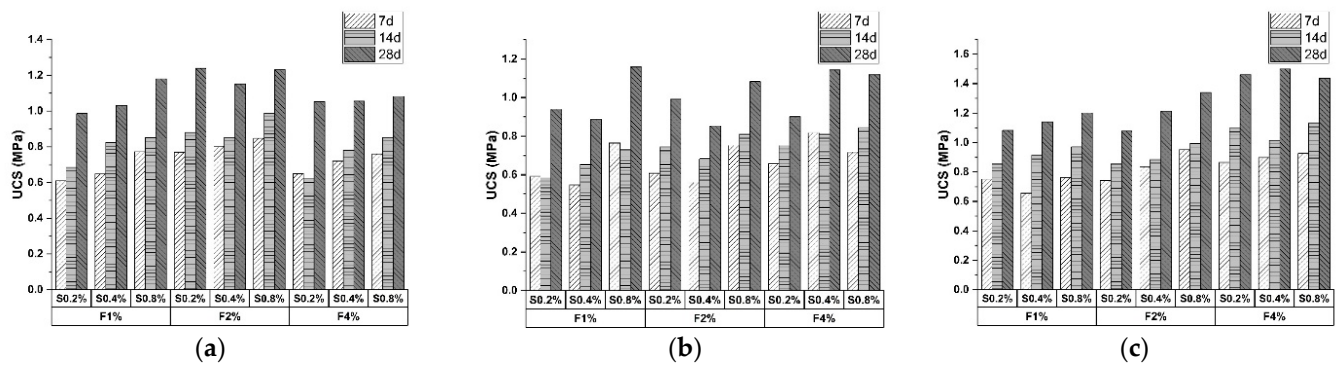
As shown in the above figures, the UCS test result increased with the increasing C&D waste percentage. The physical speculation for the performance improvement is that C&D waste demonstrates higher strength compared with soil. Particles act as support in the specimen, preventing premature collapse. Furthermore, C&D waste participates in the hydration of cement in CSS, with consequent hydration products that strengthen the material [65–67]. During the hardening process, calcium hydroxide (CH) generated by hydration serves as acidic and alkaline catalysts, respectively. The effect is to activate the hydration of silica, alumina, and old mortar in C&D waste, which produces C-S-H

to enhance sample blocks [68–70]. However, for the experimental groups with 10%, 20% and 30% cement content, the peak compressive strength increments were 54.26%, 42.23% and 9.19%, respectively. The enhancement receded with cement proportion as the binder hydration approached completion.

Previous studies have confirmed the role of sulfate as an enhancer of mechanical properties. The incorporation of sulfate alters the hydration process, leading to the retardation mechanism of ettringite formation (Equations (2) and (3)) [71,72]. The reason for the phenomenon can be attributed to the ability of C-S-H to adsorb sulfate. The uptake and release of sulfate ions lead to the rapidly accelerated rate of ettringite production and performance development occurs during late curing stage. Moreover, the formation of cement hydration products with increasing sodium sulfate mass ratio was specifically explored, as it improves CSS performance without introducing impurities. Alkali-activated SO_4^{2-} reacts with Ca^{2+} in the binder and AlO^{2-} in the liquid phase to form ettringite, which yields mechanical compensation effect [73–75]. In addition, free Na^+ form NaOH, raising the early-age pH value. Higher alkalinity fulfills the function of accelerating the dissolution of active SiO_2 and Al_2O_3, mitigating the hindrance for further ettringite formation [76–78].

$$C_3A + 3CSH_2 + 26H \rightarrow C_6AS_3H_{32} \tag{2}$$

$$2C_3A + C_6AS_3H_{32} + 4H \rightarrow 3C_4ASH_{12} \tag{3}$$
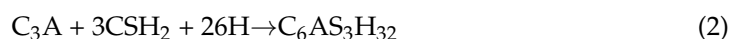
As illustrated in the figures, the UCS test results developed readily during the 14- to 28-day curing period, but slowly during the early stage. The average growth levels from 7 d to14 d and from 14 d to 28 d were 15.42% and 30.49%, respectively, a trend consistent with previous literature. However, the property alteration in this research failed to demonstrate an increasing trend. UCS showed rapid improvement from 0.2–0.8% sodium sulfate, while the durability of specimens with 0.4% sodium sulfate appeared not to be influenced by the dosing level. Compared with samples mixed with 0.2% sodium sulfate, the 0.4% proportion provided modification ranging from −14–31.36%, which indicates that the inclusion of 0.4% sodium sulfate impeded the UCS enhancement. Since the dosage was nowhere near the level of sulfate attack, the causes of the errors can be ascribed to inaccurate data recording and raw material discrepancies.

3.2. Flexural Strength Test

Figure 5 presents the flexural performance escalation of the control group due to the raising of the Portland cement proportion. It can be distinctly observed that the flexural strength increased at higher cement content (20–30%) during all curing ages. The increments ranged from 16.82–91.19% and 148.95–176.91%, respectively, for the 10–20% and 20–30% dosing levels. The maximum amplification achieved 1.94 times that for specimens with a low dosage (10–20%).
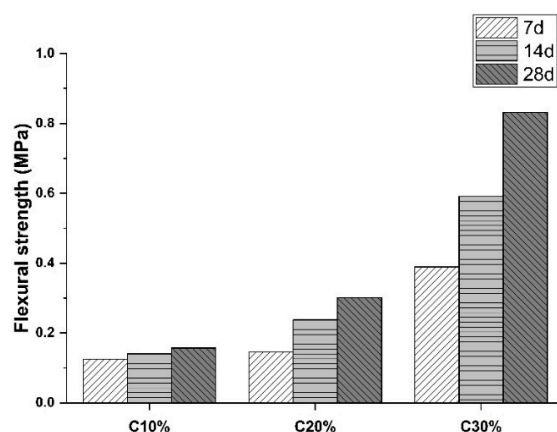

Figure 5. Flexural strength enhancement of control group (Note: C represents Portland cement).

As illustrated in Figure 6, the polypropylene fiber content demonstrated a positive effect on flexural strength growth. Mechanical properties were enhanced by up to 82.33% and 150.31% for the 1–2% and 2–4% dosing levels, respectively. Figures 7 and 8 represent the same trend, as evidenced by peak improvements in the ranges of 59.02–79.65% and 38.62–132.72%, respectively. The observation demonstrates that fibrous material contributes to flexural performance modification [79]. Specimens are therefore endowed with certain strength after the appearance of cracks, mitigating the property deterioration of weak fiber/binder ITZs [80,81]. Moreover, the maximum values of flexural strength are recorded for specimens containing 30% C&D waste and 4% fiber in Figures 6 and 7, while the peak switches to 20% C&D waste in Figure 8. The value of flexural strength then decreases from 2.03 MPa to 1.45 MPa after 30% C&D waste is added. The degeneration may be attributed to excessive C&D waste particles, which impeded the bridging effect [82]. An optimum mixture design therefore should be considered to achieve the balance between mechanical performance and material consumption.

Figure 6. Flexural strength of 10% cement specimen with (**a**) 10% C&D waste; (**b**) 20% C&D waste; (**c**) 30% C&D waste (Note: S represents sodium sulfate; F represents polypropylene fiber).
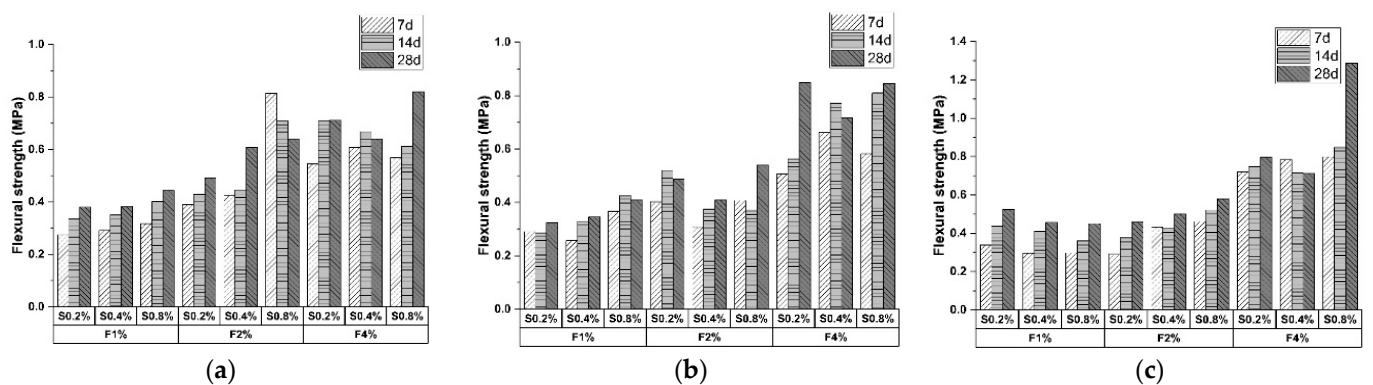
Figure 7. Flexural strength of 20% cement specimen with (**a**) 10% C&D waste; (**b**) 20% C&D waste; (**c**) 30% C&D waste (Note: S represents sodium sulfate; F represents polypropylene fiber).

The positive effect of C&D waste dosage on flexural strength can be distinctly seen from the above figures. This can be attributed to a similar reason as for the UCS results, which involved the enhancement of hydrate reaction and physical strength. However, Figure 8c illustrates deterioration, due to the increase in C&D waste leading to more large particles and entrapped air. Moreover, the peak improvements were 56.83% and 57.2%, as shown in Figures 7 and 8, while the flexural strength of the 10% cement group remained at a relatively stable level. The maximum increment in Figure 6 is 21.62%, which is 2.64 times smaller than the overall peak enhancement. This reveals that cement yields the impact of activating old mortar and improving bonding strength [83,84].
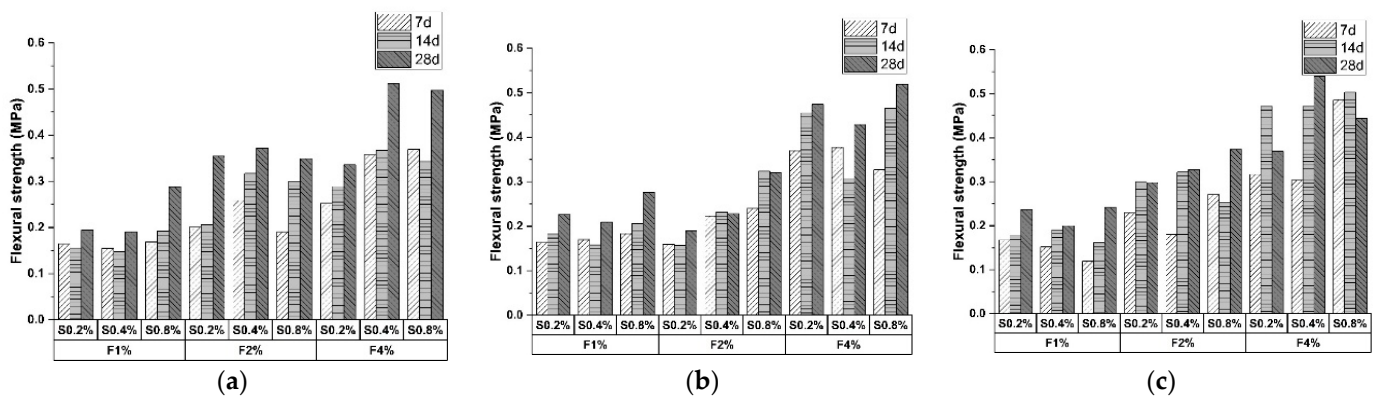
Figure 8. Flexural strength of 30% cement specimen with (**a**) 10% C&D waste; (**b**) 20% C&D waste; (**c**) 30% C&D waste (Note: S represents sodium sulfate; F represents polypropylene fiber).
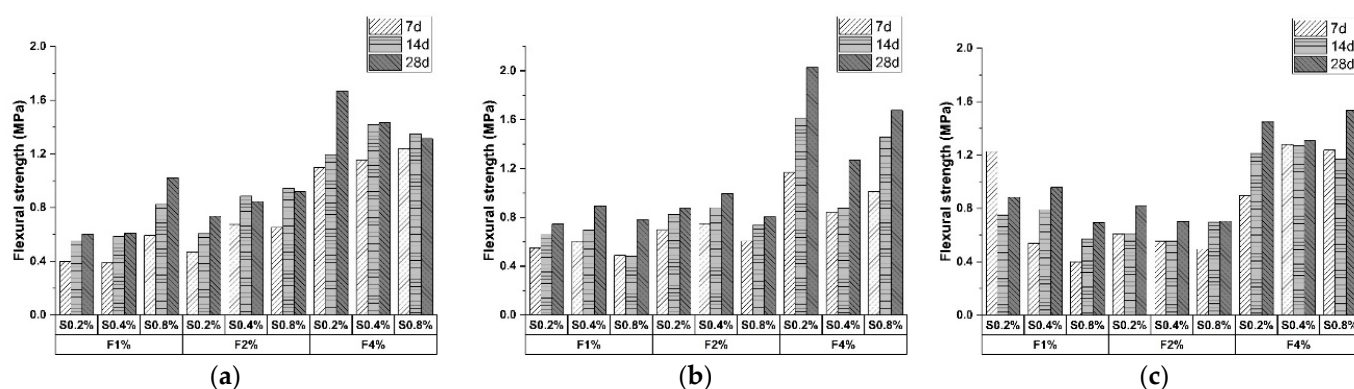
The influence of sodium sulfate dosing level is of special concern, since it has been proposed as an outstanding mechanical strength enhancer. However, as illustrated in the figures, the maximum flexural strength growth reached 69.96%, revealing that the contribution of hydration products to flexural strength is minimal. Moreover, compared with the remarkable flexural strength enhancement from the 0.2–0.8% proportion, the modification effect from the 0.2–0.4% proportion is insignificant. The source of error is similar to the reason discussed in Section 3.1.

3.3. Optimum Mixture Design

An optimum mixture design is proposed in order to seek a balance between mechanical properties and economic benefits. Tables 5 and 6 show the rankings of UCS and flexural strengths, respectively, with the inclusion of various admixtures and curing age. Combining the two tables provides a reference for the selection.

Table 5. Unconfined compressive strength ranking.

Cement	C&D Waste	Fiber	Sodium Sulfate	Curing Time (Day)	UCS (MPa)	Ranking
30%	30%	4%	0.8%	28	2.6572	1
30%	10%	1%	0.8%	28	2.5880	2
30%	10%	4%	0.8%	28	2.4336	3
30%	20%	4%	0.8%	28	2.3720	4
30%	30%	1%	0.4%	28	2.3084	5
30%	10%	2%	0.4%	28	2.2816	6
30%	30%	4%	0.8%	14	2.2656	7
30%	10%	4%	0.2%	28	2.2256	8
30%	10%	2%	0.8%	28	2.2148	9
30%	20%	2%	0.4%	28	2.1592	10

It is evidenced that 30% cement content and longer curing time are more likely to produce peak enhancement than the other combinations. As shown in Tables 5 and 6, the specimens with the top 10 enhancement levels were mixed with 30% cement, while 76.2% results were obtained after 28 days. In addition, a higher dosing level of polypropylene fiber presented a prominent performance improvement, as expressed in the tables by 15 specimens that were reinforced by 4% fiber content. It is noteworthy that the specimens ranked 1 to 4 in Table 5 were included 0.8% sodium sulfate, revealing that the effect of this inclusion tended toward maximum UCS improvement. However, the trend was not pronounced for flexural strength. Four samples in Table 6 constitute 0.2% and 0.8% sodium sulfate content, while two samples were enhanced by 0.4% proportion. Various dosages demonstrated an average influence factor on flexural resistance. C&D waste yielded a negative correlation with strength increment. Rankings in Tables 5 and 6 show that 71.4% of specimens

reinforced by a lower C&D waste proportion (10% to 20%) presented peak mechanical property enhancement. Additionally, flexural strength manifested more sensitivity to C&D waste content, as indicated in Table 6 by the sole specimens with the inclusion of 30% C&D waste that were located in lower rankings (5–10). Consequently, the specimen with variable percentages of 30%, 4%, 20% and 0.8% for Portland cement, polypropylene fiber, C&D waste, and sodium sulfate, respectively, is considered as exhibiting peak property enhancement, evidenced by its high rankings in Tables 5 and 6.

Table 6. Flexural strength ranking.

Cement	C&D Waste	Fiber	Sodium Sulfate	Curing Time (Day)	Flexural Strength (MPa)	Ranking
30%	20%	4%	0.2%	28	2.0286	1
30%	20%	4%	0.8%	28	1.6752	2
30%	10%	4%	0.2%	28	1.6690	3
30%	20%	4%	0.2%	14	1.6124	4
30%	30%	4%	0.8%	28	1.5334	5
30%	20%	4%	0.8%	14	1.4556	6
30%	30%	4%	0.2%	28	1.4504	7
30%	10%	4%	0.4%	28	1.4320	8
30%	10%	4%	0.4%	14	1.4189	9
30%	10%	4%	0.8%	14	1.3497	10

3.4. SEM Analysis

The specimen that was prepared with 30% Portland cement, 30% C&D waste, 0.4% sodium sulfate, and 4% polypropylene fiber was selected to be observed, as it demonstrated evident strength reduction. The microstructure was as presented in Figure 9a. When the specimen failed, polypropylene fiber at the section was pulled out, reflecting the strengthening mechanism of the bridging effect. Fibers were randomly distributed within the mixture, forming a spatial mesh structure that effectively reinforced the CSS [85]. However, significant porosity between particles can be readily observed, which was the major cause of undesirable mechanical performance. At a low sodium sulfate dosing level (0.4%), the over-doped fibers underwent an agglomeration effect within the slurry, and the incompletely activated cement was unable to produce sufficient amounts of hydration by-products, leading to the formation of numerous weak ITZs [86]. Figure 9b illustrates the microstructure of the specimen prepared with the aforementioned optimal mixture design. The coupling enhancement between the variables is demonstrated by the aggregates wrapped by C-S-H and ettringite. The entrapped air voids between the C&D waste and the fibers are adequately filled, resulting in promotion of ITZ strength and mechanical performance.
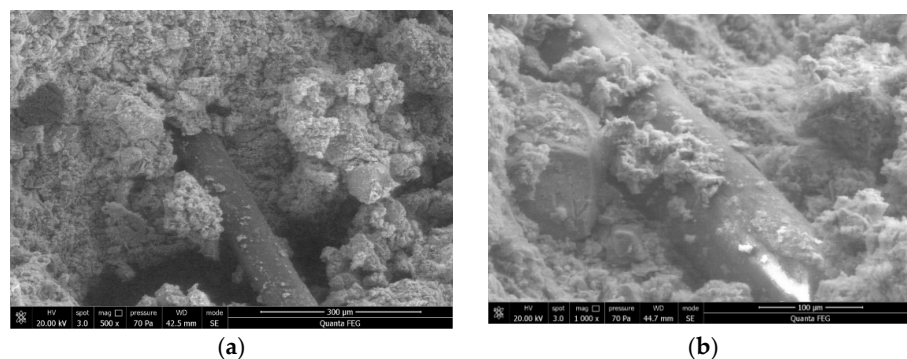

(a)   (b)

Figure 9. Microstructure of fracture surface after flexural strength test: (**a**) prior failed specimen; (**b**) optimum mixture design specimen.

　　　　Figure 10 compares microstructures of untreated polypropylene fiber with fiber used for CSS reinforcement. Ordinary polypropylene fiber represents a smooth surface, while Figure 10b illustrates the unevenness of the alkali-treated fibers. The friction provided by the crude surface enhances the particle cohesion from a physical aspect as the fibrous material cannot participate in the cement hydration [87]. Network-like polypropylene fiber therefore shows effectiveness in particle movement restriction and crack inhibition. In addition, fiber with a rougher surface yields a larger surface area for C-S-H and ettringite attachment, compensating the reduction in compactness due to fiber incorporation.
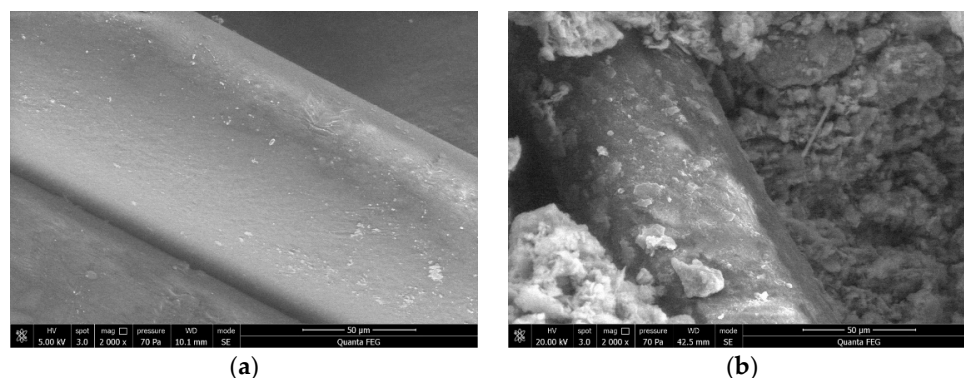

(**a**)　　　　　　　　　　　　　　　　　　　　　(**b**)

Figure 10. Microstructure of polypropylene fiber: (**a**) untreated fiber; (**b**) alkali-treated fiber.

4. Conclusions

　　　　This research conducted a series of laboratory tests to examine the enhancement of cement-stabilized soil (CSS) specimen performance with the inclusion of Portland cement, polypropylene fiber, construction and demolition (C&D) waste, and sodium sulfate. The inclusion effects on unconfined compressive strength (UCS) and flexural strength was evaluated. Primary conclusions drawn from the above analysis are summarized as follows.

　　　　(1) Portland cement hydration products raise the UCS and flexural strength results simultaneously. Ettringite presents effectiveness in enhancing physical performance, while introducing brittle failure mode.

　　　　(2) With increasing dosage of polypropylene fiber, an improvement in flexural strength is continuous, while UCS enhancement is mitigated at a 30% cement dosage.

　　　　(3) UCS and flexural strength increase with the introduction of C&D waste. The lower dosing level (10–20%) exhibits better effectivity.

　　　　(4) Mechanical properties of CSS increase with the addition of sodium sulfate content. The proportion of 0.8% derives the maximum increment. Meanwhile, 14 d–28 d curing time represents higher enhancement efficiency.

　　　　(5) Scanning electron microscope (SEM) analysis on the UCS fracture surface explained the mechanism of alkali-activated fiber reinforcement. Polypropylene fiber generates a spatial network, wrapping specimens against deformation and cracking. Sodium sulfate supplements the enhancement by catalyzing cement hydration, thus promoting the strength of the mechanical bond between fiber, aggregates, and CSS matrix.

　　　　(6) The combination of 30% Portland cement content, 4% polypropylene fiber content, 20% C&D waste content, and 0.8% sodium sulfate content is considered the optimal mixture design. By balancing the dosing level of each variable, the specimen yields the best general mechanical properties.

Author Contributions: Conceptualization, G.Z.; methodology, G.Z.; writing-original draft, Z.D.; writing-review & editing, R.Z.; project administration, R.Z.; formal analysis, C.C.; validation, C.C.; visualization, G.F.; visualization, X.L.; writing-review & editing, Y.W.; formal analysis, C.Z.; resources, C.Z. All authors have read and agreed to the published version of the manuscript.

Data Availability Statement: The data presented in this study are openly available.

Conflicts of Interest: The authors declare no conflict of interest.

Appendix A

Table A1. The Portland Cement, C&D waste, propylene fiber, and sodium sulfate proportion of the samples in this test.

ID	Portland Cement	C&D Waste	Propylene Fiber	Sodium Sulfate
Control 1	10%	NA	NA	NA
Control 2	20%	NA	NA	NA
Control 3	30%	NA	NA	NA
1				0.2%
2			1%	0.4%
3				0.8%
4				0.2%
5		10%	2%	0.4%
6				0.8%
7				0.2%
8			4%	0.4%
9				0.8%
10				0.2%
11			1%	0.4%
12				0.8%
13				0.2%
14	10%	20%	2%	0.4%
15				0.8%
16				0.2%
17			4%	0.4%
18				0.8%
19				0.2%
20			1%	0.4%
21				0.8%
22				0.2%
23		30%	2%	0.4%
24				0.8%
25				0.2%
26			4%	0.4%
27				0.8%

Table A1. *Cont.*

ID	Portland Cement	C&D Waste	Propylene Fiber	Sodium Sulfate
28				0.2%
29			1%	0.4%
30				0.8%
31		10%		0.2%
32			2%	0.4%
33				0.8%
34				0.2%
35			4%	0.4%
36				0.8%
37				0.2%
38			1%	0.4%
39				0.8%
40				0.2%
41	20%	20%	2%	0.4%
42				0.8%
43				0.2%
44			4%	0.4%
45				0.8%
46				0.2%
47			1%	0.4%
48				0.8%
49		30%		0.2%
50			2%	0.4%
51				0.8%
52				0.2%
53			4%	0.4%
54				0.8%
55				0.2%
56			1%	0.4%
57				0.8%
58				0.2%
59	30%	10%	2%	0.4%
60				0.8%
61				0.2%
62			4%	0.4%
63				0.8%

Table A1. *Cont.*

ID	Portland Cement	C&D Waste	Propylene Fiber	Sodium Sulfate
64				0.2%
65			1%	0.4%
66				0.8%
67				0.2%
68		20%	2%	0.4%
69				0.8%
70				0.2%
71			4%	0.4%
72	30%			0.8%
73				0.2%
74			1%	0.4%
75				0.8%
76				0.2%
77		30%	2%	0.4%
78				0.8%
79				0.2%
80			4%	0.4%
81				0.8%

References

1. Natianal Bureau of Statistics of China. *China Statistical Yearbook*; China Statistics Press: Beijing, China, 2019.
2. Huang, B.; Wang, X.; Kua, H.; Geng, Y.; Bleischwitz, R.; Ren, J. Construction and demolition waste management in China through the 3R principle. *Resour. Conserv. Recycl.* **2018**, *129*, 36–44. [CrossRef]
3. Construction and Demolition Waste. 2018. Available online: https://ec.europa.eu/environment/topics/waste-and-recycling/construction-and-demolition-waste_en (accessed on 1 March 2022).
4. Pacheco-Torgal, F.; Ding, Y.; Colangelo, F.; Tuladhar, R.; Koutamanis, A.D. *Advances in Construction and Demolition Waste Recycling: Management, Processing and Environmental Assessment*; Woodhead Publishing: Sawston, UK, 2020.
5. Pierrehumbert, R. There is no Plan B for dealing with the climate crisis. *Bull. At. Sci.* **2019**, *75*, 215–221. [CrossRef]
6. Pierrehumbert, R. How to decarbonize? Look to Sweden. *Bull. At. Sci.* **2016**, *72*, 105–111. [CrossRef]
7. Alley, R.B.; Marotzke, J.; Nordhaus, W.D.; Overpeck, J.T.; Peteet, D.M.; Pielke, R.A., Jr.; Pierrehumbert, R.T.; Rhines, P.B.; Stocker, T.F.; Talley, L.D.; et al. Abrupt Climate Change. *Science* **2003**, *299*, 2005–2010. [CrossRef]
8. Jellinek, A.M.; Lenardic, A.; Pierrehumbert, R. Earth's supecontinental climate control. In *EGU General Assembly Conference Abstracts*; European Geosciences Union: Munich, Germany, 2021.
9. Liu, C.; Wu, D.; Li, Y.; Du, Y. Large-scale pavement roughness measurements with vehicle crowdsourced data using semi-supervised learning. *Transp. Res. Part C Emerg. Technol.* **2021**, *125*, 103048. [CrossRef]
10. Li, X.; Li, Y.; Jia, T.; Zhou, L.; Hijazi, I.H. The six dimensions of built environment on urban vitality: Fusion evidence from multi-source data. *Cities* **2021**, *121*, 103482. [CrossRef]
11. Ghouleh, Z.; Shao, Y. Turning municipal solid waste incineration into a cleaner cement production. *J. Clean. Prod.* **2018**, *195*, 268–279. [CrossRef]
12. Zhu, W.; Chen, X.; Struble, L.J.; Yang, E.-H. Characterization of calcium-containing phases in alkali-activated municipal solid waste incineration bottom ash binder through chemical extraction and deconvoluted Fourier transform infrared spectra. *J. Clean. Prod.* **2018**, *192*, 782–789. [CrossRef]
13. García-Taengua, E.; Sonebi, M.; Crossett, P.; Taylor, S.; Deegan, P.; Ferrara, L.; Pattarini, A. Performance of sustainable SCC mixes with mineral additions for use in precast concrete industry. *J. Sustain. Cem. Mater.* **2015**, *5*, 157–175. [CrossRef]
14. Sun, J.; Wang, Y.; Liu, S.; Dehghani, A.; Xiang, X.; Wei, J.; Wang, X. Mechanical, chemical and hydrothermal activation for waste glass reinforced cement. *Constr. Build. Mater.* **2021**, *301*, 124361. [CrossRef]
15. Tang, Y.; Feng, W.; Chen, Z.; Nong, Y.; Guan, S.; Sun, J. Fracture behavior of a sustainable material: Recycled concrete with waste crumb rubber subjected to elevated temperatures. *J. Clean. Prod.* **2021**, *318*, 128553. [CrossRef]

16. Wang, B.; Yan, L.; Fu, Q.; Kasal, B. A Comprehensive Review on Recycled Aggregate and Recycled Aggregate Concrete. *Resour. Conserv. Recycl.* **2021**, *171*, 105565. [CrossRef]

17. Tayeh, B.A.; Alsaffar, D.; Alyousef, R. The Utilization of Recycled Aggregate in High Performance Concrete: A Review. *J. Mater. Res. Technol.* **2020**, *9*, 8469–8481. [CrossRef]

18. del Valle-Zermeño, R.; Giro-Paloma, J.; Formosa, J.; Chimenos, J.M. APC Fly Ash Recycling: Development of a Granular Material from Laboratory to a Pilot Scale. *Waste Biomass Valorization* **2017**, *8*, 1409–1419. [CrossRef]

19. Toraldo, E.; Saponaro, S.F. A road pavement full-scale test track containing stabilized bottom ashes. *Environ. Technol.* **2014**, *36*, 1114–1122. [CrossRef]

20. Huang, H.; Xue, C.; Zhang, W.; Guo, M. Torsion design of CFRP-CFST columns using a data-driven optimization approach. *Eng. Struct.* **2021**, *251*, 113479. [CrossRef]

21. Guo, Z.; Tu, A.; Chen, C.; Lehman, D.E. Mechanical properties, durability, and life-cycle assessment of concrete building blocks incorporating recycled concrete aggregates. *J. Clean. Prod.* **2018**, *199*, 136–149. [CrossRef]

22. Liu, J.; Wu, C.; Wu, G.; Wang, X. A novel differential search algorithm and applications for structure design. *Appl. Math. Comput.* **2015**, *268*, 246–269. [CrossRef]

23. Xu, H.; Wang, X.-Y.; Liu, C.-N.; Chen, J.-N.; Zhang, C. A 3D root system morphological and mechanical model based on L-Systems and its application to estimate the shear strength of root-soil composites. *Soil Tillage Res.* **2021**, *212*, 105074. [CrossRef]

24. Wen, P.; Wang, C.; Song, L.; Niu, L.; Chen, H. Durability and Sustainability of Cement-Stabilized Materials Based on Utilization of Waste Materials: A Literature Review. *Sustainability* **2021**, *13*, 11610. [CrossRef]

25. Ifediniru, C.; Ekeocha, N.E. Performance of cement-stabilized weak subgrade for highway embankment construction in Southeast Nigeria. *Int. J. Geo-Eng.* **2022**, *13*, 1. [CrossRef]

26. Dahale, P.P.; Nagarnaik, P.B.; Gajbhiye, A.R. Utilization of solid waste for soil stabilization: A review. *Electron. J. Geotech. Eng.* **2012**, *17*, 2443–2461.

27. Islam, M.S.; Elahi, T.E.; Shahriar, A.R.; Mumtaz, N. Effectiveness of fly ash and cement for compressed stabilized earth block construction. *Constr. Build. Mater.* **2020**, *255*, 119392. [CrossRef]

28. Kariyawasam, K.; Jayasinghe, C. Cement stabilized rammed earth as a sustainable construction material. *Constr. Build. Mater.* **2016**, *105*, 519–527. [CrossRef]

29. Anagnostopoulos, C.A. Strength properties of an epoxy resin and cement-stabilized silty clay soil. *Appl. Clay Sci.* **2015**, *114*, 517–529. [CrossRef]

30. Donatello, S.; Fernández-Jimenez, A.; Palomo, A. Very high volume fly ash cements. Early age hydration study using Na 2 SO 4 as an activator. *J. Am. Ceram. Soc.* **2013**, *96*, 900–906. [CrossRef]

31. Huang, Y.; An, C.; Zhang, Q.; Zang, L.; Shao, H.; Liu, Y.; Zhang, Y.; Yuan, H.; Wang, C.; Wang, Y. Cost-effective mechanochemical synthesis of highly dispersed supported transition metal catalysts for hydrogen storage. *Nano Energy* **2020**, *80*, 105535. [CrossRef]

32. Huang, L.; Yang, Z. Early hydration of tricalcium silicate with potassium hydroxide and sulfate from pore solution and solid view. *Constr. Build. Mater.* **2019**, *230*, 116988. [CrossRef]

33. Atashband, S.; Sabermahani, M.; Elahi, H. Internal and External Effects of Sodium Sulfate on the Strength of Soil Cement. *Iran. J. Sci. Technol. Trans. Civ. Eng.* **2020**, *45*, 2595–2610. [CrossRef]

34. Tsai, Y.-H.; Wang, J.; Chien, W.-T.; Wei, C.-Y.; Wang, X.; Hsieh, S.-H. A BIM-based approach for predicting corrosion under insulation. *Autom. Constr.* **2019**, *107*, 102923. [CrossRef]

35. Tang, Z.; Li, W.; Ke, G.; Zhou, J.L.; Tam, V.W. Sulfate attack resistance of sustainable concrete incorporating various industrial solid wastes. *J. Clean. Prod.* **2019**, *218*, 810–822. [CrossRef]

36. Firoozi, A.A.; Guney Olgun, C.; Firoozi, A.A.; Baghini, M.S. Fundamentals of soil stabilization. *Int. J. Geo-Eng.* **2017**, *8*, 26. [CrossRef]

37. Sharma, L.; Sirdesai, N.; Sharma, K.; Singh, T. Experimental study to examine the independent roles of lime and cement on the stabilization of a mountain soil: A comparative study. *Appl. Clay Sci.* **2018**, *152*, 183–195. [CrossRef]

38. Wu, C.; Wang, X.; Chen, M.; Kim, M.J. Differential received signal strength based RFID positioning for construction equipment tracking. *Adv. Eng. Inform.* **2019**, *42*, 100960. [CrossRef]

39. Wang, L.; Roy, A.; Seals, R.K.; Byerly, Z. Suppression of Sulfate Attack on a Stabilized Soil. *J. Am. Ceram. Soc.* **2005**, *88*, 1600–1606. [CrossRef]

40. Xu, S.; Wang, J.; Shou, W.; Ngo, T.; Sadick, A.-M.; Wang, X. Computer Vision Techniques in Construction: A Critical Review. *Arch. Comput. Methods Eng.* **2020**, *28*, 3383–3397. [CrossRef]

41. Zhang, W.; Wu, C.; Zhong, H.; Li, Y.; Wang, L. Prediction of undrained shear strength using extreme gradient boosting and random forest based on Bayesian optimization. *Geosci. Front.* **2020**, *12*, 469–477. [CrossRef]

42. Sun, J.; Wang, Y.; Yao, X.; Ren, Z.; Zhang, G.; Zhang, C.; Chen, X.; Ma, W.; Wang, X. Machine-Learning-Aided Prediction of Flexural Strength and ASR Expansion for Waste Glass Cementitious Composite. *Appl. Sci.* **2021**, *11*, 6686. [CrossRef]

43. Sun, J.; Ma, Y.; Li, J.; Zhang, J.; Ren, Z.; Wang, X. Machine learning-aided design and prediction of cementitious composites containing graphite and slag powder. *J. Build. Eng.* **2021**, *43*, 102544. [CrossRef]

44. Sun, Y.; Li, G.; Zhang, J.; Sun, J.; Xu, J. Development of an Ensemble Intelligent Model for Assessing the Strength of Cemented Paste Backfill. *Adv. Civ. Eng.* **2020**, *2020*, 1–6. [CrossRef]

45. Zhang, C.; Kordestani, H.; Masri, S.F.; Wang, J.; Sun, L. Data-driven system parameter change detection for a chain-like uncertainties embedded structure. *Struct. Control Heal. Monit.* **2021**, *28*, e2821. [CrossRef]

46. Cristelo, N.; Cunha, V.M.; Dias, M.; Gomes, A.T.; Miranda, T.; Araújo, N. Influence of discrete fibre reinforcement on the uniaxial compression response and seismic wave velocity of a cement-stabilised sandy-clay. *Geotext. Geomembr.* **2015**, *43*, 1–13. [CrossRef]

47. Kumar, A.; Walia, B.S.; Mohan, J. Compressive strength of fiber reinforced highly compressible clay. *Constr. Build. Mater.* **2006**, *20*, 1063–1068. [CrossRef]

48. Aslani, F.; Sun, J.; Bromley, D.; Ma, G. Fiber-reinforced lightweight self-compacting concrete incorporating scoria aggregates at elevated temperatures. *Struct. Concr.* **2019**, *20*, 1022–1035. [CrossRef]

49. Wang, J.; Dai, Q.; Si, R.; Guo, S. Investigation of properties and performances of Polyvinyl Alcohol (PVA) fiber-reinforced rubber concrete. *Constr. Build. Mater.* **2018**, *193*, 631–642. [CrossRef]

50. Wang, J.; Dai, Q.; Si, R.; Ma, Y.; Guo, S. Fresh and mechanical performance and freeze-thaw durability of steel fiber-reinforced rubber self-compacting concrete (SRSCC). *J. Clean. Prod.* **2020**, *277*, 123180. [CrossRef]

51. Dobrovolski, M.E.; Munhoz, G.S.; Pereira, E.; Medeiros-Junior, R.A. Effect of crystalline admixture and polypropylene microfiber on the internal sulfate attack in Portland cement composites due to pyrite oxidation. *Constr. Build. Mater.* **2021**, *308*, 125018. [CrossRef]

52. Wang, J.; Dai, Q.; Guo, S.; Si, R. Study on Rubberized Concrete Reinforced with Different Fibers. *ACI Mater. J.* **2019**, *116*, 21–31. [CrossRef]

53. Yu, X.; Sun, Y.; Zhao, D.; Wu, S. A revised contact stiffness model of rough curved surfaces based on the length scale. *Tribol. Int.* **2021**, *164*, 107206. [CrossRef]

54. China MoHaU-RDotPsRo (Ed.) *Standard for Soil Test Method, in GB/T 50123-1999*; Planning Press: Beijing, China, 1999.

55. Sun, J.; Huang, Y.; Aslani, F.; Wang, X.; Ma, G. Mechanical enhancement for EMW-absorbing cementitious material using 3D concrete printing. *J. Build. Eng.* **2021**, *41*, 102763. [CrossRef]

56. Zhang, W.; Li, H.; Li, Y.; Liu, H.; Chen, Y.; Ding, X. Application of deep learning algorithms in geotechnical engineering: A short critical review. *Artif. Intell. Rev.* **2021**, *54*, 5633–5673. [CrossRef]

57. Amini, O.; Ghasemi, M. Laboratory study of the effects of using magnesium slag on the geotechnical properties of cement stabilized soil. *Constr. Build. Mater.* **2019**, *223*, 409–420. [CrossRef]

58. Feng, J.; Chen, B.; Sun, W.; Wang, Y. Microbial induced calcium carbonate precipitation study using Bacillus subtilis with application to self-healing concrete preparation and characterization. *Constr. Build. Mater.* **2021**, *280*, 122460. [CrossRef]

59. Wang, M.; Yang, X.; Wang, W. Establishing a 3D aggregates database from X-ray CT scans of bulk concrete. *Constr. Build. Mater.* **2021**, *315*, 125740. [CrossRef]

60. Singh, V.; Gu, N.; Wang, X. A theoretical framework of a BIM-based multi-disciplinary collaboration platform. *Autom. Constr.* **2011**, *20*, 134–144. [CrossRef]

61. Xu, J.; Wu, Z.; Chen, H.; Shao, L.; Zhou, X.; Wang, S. Triaxial Shear Behavior of Basalt Fiber-Reinforced Loess Based on Digital Image Technology. *KSCE J. Civ. Eng.* **2021**, *25*, 3714–3726. [CrossRef]

62. Sun, J.; Aslani, F.; Lu, J.; Wang, L.; Huang, Y.; Ma, G. Fibre-reinforced lightweight engineered cementitious composites for 3D concrete printing. *Ceram. Int.* **2021**, *47*, 27107–27121. [CrossRef]

63. Aslani, F.; Sun, J.; Huang, G. Mechanical Behavior of Fiber-Reinforced Self-Compacting Rubberized Concrete Exposed to Elevated Temperatures. *J. Mater. Civ. Eng.* **2019**, *31*, 04019302. [CrossRef]

64. Hou, L.; Wu, S.; Zhang, G.; Tan, Y.; Wang, X. Literature Review of Digital Twins Applications in Construction Workforce Safety. *Appl. Sci.* **2020**, *11*, 339. [CrossRef]

65. Dimitriou, G.; Savva, P.; Petrou, M.F. Enhancing mechanical and durability properties of recycled aggregate concrete. *Constr. Build. Mater.* **2018**, *158*, 228–235. [CrossRef]

66. Xiang, G.X.; Xiang, G.X.; Gao, X.; Gao, X.; Tang, W.J.; Tang, W.J.; Jie, X.Z.; Jie, X.Z.; Huang, X.; Huang, X. Numerical study on transition structures of oblique detonations with expansion wave from finite-length cowl. *Phys. Fluids* **2020**, *32*, 056108. [CrossRef]

67. Zhang, H.; Liu, Y.; Deng, Y. Temperature gradient modeling of a steel box-girder suspension bridge using Copulas probabilistic method and field monitoring. *Adv. Struct. Eng.* **2020**, *24*, 947–961. [CrossRef]

68. Cheng, H.L.; Wang, C.Y. The influence of sodium silicate on the properties of recycled aggregate. *Gypsum Cem. Build.* **2005**, *12*, 12–14.

69. Tam, V.W.; Soomro, M.; Evangelista, A.C.J. A review of recycled aggregate in concrete applications (2000–2017). *Constr. Build. Mater.* **2018**, *172*, 272–292. [CrossRef]

70. Nanayakkara, O.; Gunasekara, C.; Sandanayake, M.; Law, D.W.; Nguyen, K.; Xia, J.; Setunge, S. Alkali activated slag concrete incorporating recycled aggregate concrete: Long term performance and sustainability aspect. *Constr. Build. Mater.* **2020**, *271*, 121512. [CrossRef]

71. Joseph, S.; Skibsted, J.; Cizer, Ö. A quantitative study of the C3A hydration. *Cem. Concr. Res.* **2018**, *115*, 145–159. [CrossRef]

72. Zhao, R.; Zhang, L.; Guo, B.; Chen, Y.; Fan, G.; Jin, Z.; Guan, X.; Zhu, J. Unveiling substitution preference of chromium ions in sulphoaluminate cement clinker phases. *Compos. Part B Eng.* **2021**, *222*, 109092. [CrossRef]

73. Marchon, D.; Flatt, R.J. *Mechanisms of Cement Hydration, in Science and Technology of Concrete Admixtures*; Elsevier: Amsterdam, The Netherlands, 2016; pp. 129–145.

74. Liu, B.; Spiekermann, R.; Zhao, C.; Püttmann, W.; Sun, Y.; Jasper, A.; Uhl, D. Evidence for the repeated occurrence of wildfires in an upper Pliocene lignite deposit from Yunnan, SW China. *Int. J. Coal Geol.* **2022**, *250*, 103924. [CrossRef]

75. Wang, L.; Yuan, J.; Wu, C.; Wang, X. Practical algorithm for stochastic optimal control problem about microbial fermentation in batch culture. *Optim. Lett.* **2017**, *13*, 527–541. [CrossRef]

76. Mähler, J.; Persson, I. A Study of the Hydration of the Alkali Metal Ions in Aqueous Solution. *Inorg. Chem.* **2011**, *51*, 425–438. [CrossRef]

77. Huang, L.; Yan, P. Effect of alkali content in cement on its hydration kinetics and mechanical properties. *Constr. Build. Mater.* **2019**, *228*, 116833. [CrossRef]

78. Salvador, R.P.; Cavalaro, S.H.; Segura, I.; Figueiredo, A.D.; Pérez, J. Early age hydration of cement pastes with alkaline and alkali-free accelerators for sprayed concrete. *Constr. Build. Mater.* **2016**, *111*, 386–398. [CrossRef]

79. Xiao, X.; Bu, G.; Ou, Z.; Li, Z. Nonlinear in-plane instability of the confined FGP arches with nanocomposites reinforcement under radially-directed uniform pressure. *Eng. Struct.* **2021**, *252*, 113670. [CrossRef]

80. Zhang, W.; Tang, Z. Numerical Modeling of Response of CFRP–Concrete Interfaces Subjected to Fatigue Loading. *J. Compos. Constr.* **2021**, *25*, 04021043. [CrossRef]

81. Wang, J.; Dai, Q.; Si, R. Experimental and Numerical Investigation of Fracture Behaviors of Steel Fiber–Reinforced Rubber Self-Compacting Concrete. *J. Mater. Civ. Eng.* **2022**, *34*, 04021379. [CrossRef]

82. Shi, T.; Lan, Y.; Hu, Z.; Wang, H.; Xu, J.; Zheng, B. Tensile and Fracture Properties of Silicon Carbide Whisker-Modified Cement-Based Materials. *Int. J. Concr. Struct. Mater.* **2022**, *16*, 2. [CrossRef]

83. Sun, J.; Lin, S.; Zhang, G.; Sun, Y.; Zhang, J.; Chen, C.; Morsy, A.M.; Wang, X. The effect of graphite and slag on electrical and mechanical properties of electrically conductive cementitious composites. *Constr. Build. Mater.* **2021**, *281*, 122606. [CrossRef]

84. Li, J.; Qin, Q.; Sun, J.; Ma, Y.; Li, Q. Mechanical and conductive performance of electrically conductive cementitious composite using graphite, steel slag, and GGBS. *Struct. Concr.* **2020**, *22*, 1–15. [CrossRef]

85. Wang, J.; Dai, Q.; Si, R.; Guo, S. Mechanical, durability, and microstructural properties of macro synthetic polypropylene (PP) fiber-reinforced rubber concrete. *J. Clean. Prod.* **2019**, *234*, 1351–1364. [CrossRef]

86. Aslani, F.; Hou, L.; Nejadi, S.; Sun, J.; Abbasi, S. Experimental analysis of fiber-reinforced recycled aggregate self-compacting concrete using waste recycled concrete aggregates, polypropylene, and steel fibers. *Struct. Concr.* **2019**, *20*, 1670–1683. [CrossRef]

87. Xu, J.; Wu, Z.; Chen, H.; Shao, L.; Zhou, X.; Wang, S. Study on Strength Behavior of Basalt Fiber-Reinforced Loess by Digital Image Technology (DIT) and Scanning Electron Microscope (SEM). *Arab. J. Sci. Eng.* **2021**, *46*, 11319–11338. [CrossRef]